5TH IAA Conference on Space Situational Awareness (ICSSA)

Tres Cantos - Madrid, Spain

IAA-ICSSA-26-04

ROTATIONAL DECELERATION OF SPACE OBJECTS USING ORBITAL LASERS

Dennis Baral(1), **Stefan Scharring**(2), **Thomas Klumpp**(3)
(1) German Aerospace Center, Pfaffenwaldring 38 - 40, 70569 Stuttgart, +49 711 6862 8290, dennis.baral@dlr.de
(2) German Aerospace Center, Pfaffenwaldring 38 - 40, 70569 Stuttgart, +49 711 6862 517, stefan.scharring@dlr.de
(3) German Aerospace Center, Pfaffenwaldring 38 - 40, 70569 Stuttgart, +49 711 6862 8604, thomas.klumpp@dlr.de

Keywords: *space debris removal, de-spinning, laser ablation, simulation, ray tracing*

The growing population of space debris in low Earth orbit (LEO) poses increasing risks to operational spacecrafts and long-term spaceflight sustainability. Active Debris Removal (ADR) of uncooperative, fast-spinning objects remains particularly challenging due to constraints from robotic capture dynamics. This work investigates laser-ablative de-tumbling as a contactless method to reduce angular momentum and enable subsequent capture.

A key contribution of this research is the definition of key laser parameters suitable for de-spinning applications such as wavelength, pulse energy, repetition rate, pulse length, beam divergence, and beam quality. These parameters are critical for predicting and optimizing laser-matter interactions for representative debris materials. Building on this, an existing laser-matter interaction simulation framework was extensively redeveloped.

The software features ray tracing accelerated with a graphical processing unit (GPU), advanced beam caustic modelling, individual beam intensity profiles and multi-material target handling. To calculate the angular momentum imparted by laser pulses, the framework combines simulated surface fluence with empirically measured and simulated material response data. Significantly, the de-spinning simulations now incorporate technical tolerances and real-world uncertainties, including laser jitter, pointing precision limits, and servicer and target position uncertainties, enabling more realistic mission analyses.

The extended framework was applied to simulate de-tumbling of representative satellites and debris objects in LEO using real-world geometric and inertial data. Results demonstrate that complete rotational deceleration is achievable within mission-relevant timescales, while also revealing the effects of operational constraints, optimal irradiation strategies, and targeting uncertainties. Beyond demonstrating feasibility, the simulation framework provides mission-relevant predictions, such as de-spinning duration and laser energy requirements, across multiple target scenarios.

These results offer critical insights for servicer design, mission planning, and operational optimization, establishing laser-ablative de-tumbling as a technically viable key

method to enable ADR of fast-spinning or tumbling objects. This work bridges the gap between theoretical modeling and potential in-orbit demonstrations, providing a quantitative tool for risk assessment and mission design in debris removal operations, laying the ground for further developments towards a digital twin for in-orbit operations.

1. Introduction

The accumulation of orbital debris in low Earth orbit (LEO) has become a critical threat to sustainable space operations. In particular, fast-spinning, uncooperative objects pose severe challenges for conventional robotic capture systems. Laser-ablative de-spinning offers a contactless alternative by exploiting photon-induced material ablation to generate thrust and reduce angular momentum.
This paper aims to validate the feasibility of laser-ablative de-spinning in combination with realistic and existing laser parameters, measured or simulated material parameters and target objects with measured spins. We employ a self-developed ray tracing software to simulate the laser-matter interactions for given laser, material and object parameters. This software models the interaction between a pulsed laser system and a rigid body with a given angular impulse and corresponding angular velocity. The laser beam is modeled as a bundle of rays. A detailed description of the used software is found in [1], while the current version of this software employs two significant new features. We integrated a secondary model that adds systematic disturbances to the system, that is used to simulate a beam pointing jitter. We also implemented an initial optimization method to guide the laser beam to advantageously irradiate the target and reduce the total de-spinning time. By designing a merit function, it is defined which results are considered as advantageous for the de-spinning process.
The results provide significant insights into the feasibility of laser-ablative de-spinning dynamics. The software enables estimation of de-spinning duration and servicer power consumption, and provides insights and constraints for mission and servicer design.

2. Laser-Ablative Momentum Transfer

A laser that creates sufficiently high energy density on a target surface can induce material ablation. The ablated material is ejected from the surface at high velocity, generating a target momentum by recoil. This impulse can be harnessed for momentum transfer applications, such as de-spinning space debris. The momentum transfer per laser pulse depends on the combination of laser, material and geometric properties. Some of the key parameters that influence the resulting impulse are, according to [2, 3], the surface material, fluence and roughness, the incidence angle and the laser parameters, such as wavelength, pulse length and the pulse energy. The concept of impulse coupling coefficient c_m, as described in [4], is often used. This coefficient fundamentally relates the incident laser energy E_L to the generated impulse p as

$$c_\mathrm{m} = \frac{\Delta p}{E_\mathrm{L}} = \frac{\mu_m v_E}{\Phi_L}. \tag{1}$$

Here, μ_m is the mass density of the ablated area and v_E is the exhaust velocity of the ablated material. The incident laser fluence Φ_L is defined as the laser energy per laser profile area. The momentum coupling coefficient c_m has the unit of $\mathrm{N\,s/J}$. It can be interpreted as the efficiency of the available laser energy to generated impulse. Higher

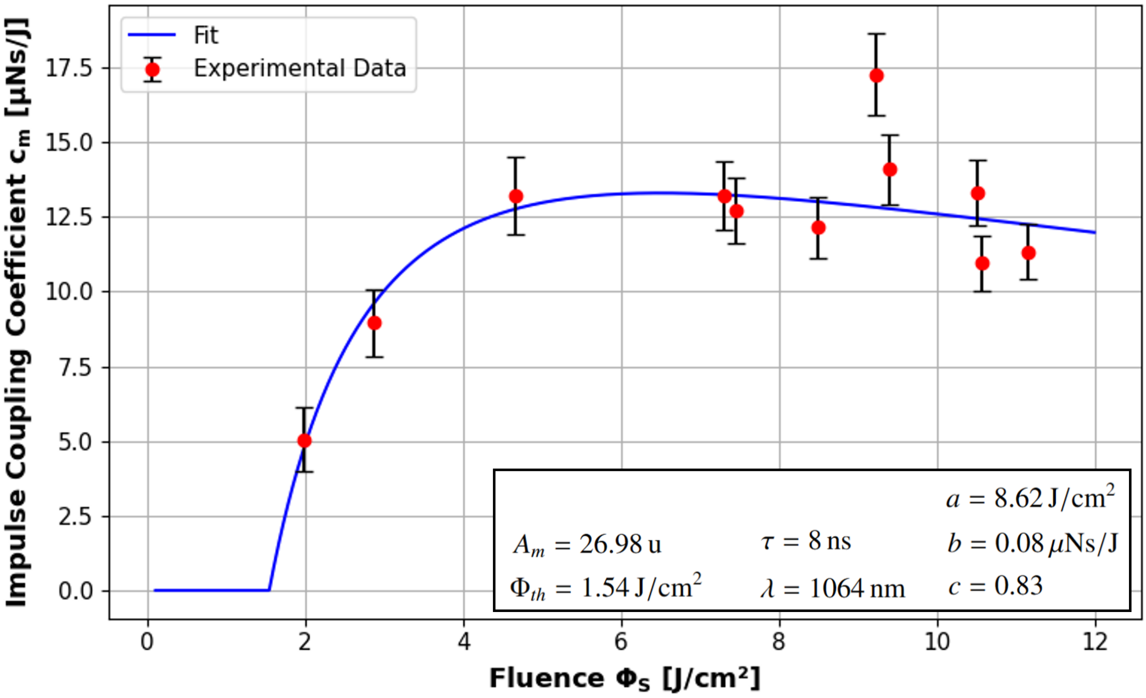

Figure 1: Impulse coupling coefficient c_m for aluminum as a function of incident surface laser fluence Φ_S. This fit is based on data from [6] and used in the simulation software. A laser with $1064\,\mathrm{nm}$ wavelength and a pulse length of $8\,\mathrm{ns}$ is used.

values of c_m indicate more efficient momentum transfer, as more impulse is generated for a given amount of laser energy. The impulse coupling coefficient is dependent on the material and laser parameters. Its value is often empirically measured for multiple surface fluences on the target material. For the current simulation, the fit function from [5] is used.

$$c_m(\Phi_S) \approx \begin{cases} \dfrac{\Phi_S - \Phi_{th}}{a + \Phi_S - \Phi_{th}} \cdot b \cdot A_m^{\frac{7}{16}} \cdot \left(\dfrac{\sqrt{\tau}}{\lambda \Phi_S} \cdot \left[\frac{m \cdot J}{\sqrt{s} \cdot cm^2} \right] \right)^c, & \Phi_S > \Phi_{th} \\ 0, & \Phi_S \leq \Phi_{th} \end{cases} \tag{2}$$

This fit uses empirically retrieved fit parameters a, b, c and the ablation threshold fluence Φ_{th}. This fluence Φ_{th} is the minimum fluence required to start ablation on the target surface. For aluminum this threshold is approximately at $1.54\,\mathrm{J/cm^2}$ with $1064\,\mathrm{nm}$ wavelength and a pulse length of $8\,\mathrm{ns}$. Below this threshold no impulse is generated by ablation on the target. A_m is defined as the atomic mass of the target material. The last factor models the decrease of c_m for high surface fluences, which is caused by plasma shielding effects. This is influenced by the laser wavelength λ and the pulse length τ_L. Figure 1 shows qualitatively typical values for the impulse coupling coefficient. Below the ablation threshold no impulse is generated. Just above the threshold c_m increases rapidly with increasing surface fluence. After reaching a peak value, c_m decreases again for high surface fluences due to plasma shielding effects. The direction of the generated impulse is always normal to the irradiated surface.

3. Laser Parameters for Ablative De-Spinning in Orbit

The requirements for laser systems operating in space are significantly more restrictive than for terrestrial applications. Vacuum operation, ionizing radiation, launch-induced vibrations, and extreme thermal cycling demand highly optimized and robust laser architectures. The following subsections outline the laser parameters required for laser ablation-based de-spinning in orbit and compares them to those of already deployed spaceborne systems.

Current spaceborne laser systems are primarily deployed for remote sensing, like light imaging, detection and ranging (LIDAR) and communication. To date, no dedicated laser-ablative impulse transfer systems operate in orbit. However, spaceborne lidar missions already possess laser parameters sufficient for ablation-based de-spinning when appropriately focused and at a relatively close distance ($< 100\,\mathrm{m}$). An overview of LIDAR systems is provided in [7]. Representative examples include the ICESat, CALIPSO, and Aeolus missions, whose laser specifications are summarized in Table 1. All listed systems employ solid-state neodymium-doped yttrium aluminum garnet

Table 1: Key parameters of selected spaceborne laser LIDAAR missions from [7] (*[8], **[9], *[10]). The higher energy value per pulse counts for only the fundamental laser wavelength.**

Mission	Pulse rate (Hz)	Pulse length (ns)	Energy per pulse (mJ)	Wavelength (nm)
ICESat	40	4*	100	1064 / 532
CALIPSO	20	20**	110 (220)**	1064 / 532
Aeolus	51	20***	110 (420)***	355

(Nd:YAG) lasers. These lasers produce light at 1064nm. This is the fundamental laser wavelength. ICESat and CALIPSO utilize second-harmonic generation, where additional components of the laser reduce the wavelength to 532 nm. Aeolus additionally employs third-harmonic generation to further reduce the wavelength to 355 nm. Although wavelength flexibility can improve ablation efficiency for heterogeneous targets through optimized surface absorptivity, harmonic generation of smaller wavelengths inherently reduces the pulse energy. Multiple wavelengths are not strictly required for laser ablation. The pulse energies of the listed systems, when combined with realistic beam focusing, are sufficient to exceed typical ablation thresholds Φ_{th} for metals, polymers and other material types. In the following, we provide and an illustrative example of the laser parameters required for laser ablation-based de-spinning in orbit. The incident laser fluence Φ at the target surface is given by

$$w_0 = \sqrt{\frac{E_{\mathrm{p}} \cdot \cos(i)}{\pi \cdot \Phi_{\mathrm{th}}}}, \tag{3}$$

where E_{p} is the pulse energy, w_0 is the beam waist radius at the focus plane and i is the incidence angle. For a pulse energy of $E_{\mathrm{p}} = 420\,\mathrm{mJ}$ (like the AEOLUS laser at its fundamental wavelength) we can calculate the required spot radius on the surface to create sufficient fluence for ablation. For aluminum the ablation threshold is assumed with $1.54\,\mathrm{J/cm^2}$. This corresponds to measurements in [6]. Depending on the surface roughness, this ablation threshold can change significantly together with the impulse coupling coefficient [11]. With Equation 3, we get a minimal required spot radius w_0 of $2.95\,\mathrm{mm}$ at the surface for a normal incidence. With an incidence angle of 60° the required spot radius reduces to $w_0 = 2.08\,\mathrm{mm}$. Further we assume a distance of $80\,\mathrm{m}$ to the target. To achieve an impulse coupling coefficient close to its maximum at $\Phi_S = 6.5\,\mathrm{J/cm^2}$, a focus waist of approximately $w_0 \approx 1.43\,\mathrm{mm}$ is needed. Based on the diffraction limit of this beam we can calculate the required exit aperture of the laser system with the beam divergence angle θ_{div}

$$\theta_{\mathrm{div}} = \frac{M^2 \cdot \lambda}{\pi \cdot w_0} \approx 0.237\,\mathrm{mrad}. \tag{4}$$

The beam quality factor M^2 quantifies deviation from an ideal Gaussian beam $M^2 = 1$. Optical aberrations increase M^2, requiring a larger beam diameter at the aperture to maintain the focus waist. Assuming $M^2 = 2$, the aperture waist radius is $40\,\mathrm{mm}$. To mitigate significant power loss due to beam clipping at the aperture, an aperture radius of at least $100\,\mathrm{mm}$ is recommended to accommodate the full beam profile. This is technically feasible through the use of a beam expander, which increases the beam diameter before focusing, thereby reducing divergence and enabling the use of shorter focal length optics. Such a configuration ensures compatibility with practical optical systems while maintaining sufficient beam quality for the intended application.

As discussed in [12], nanosecond-scale laser pulses predominantly cause ablation through melting and subsequent vaporization. Shorter pulses (typically $< 100\,\mathrm{ps}$) invoke ablation mechanisms like spallation or phase explosion. For aluminum, longer pulses achieve higher specific impulses, respectively a higher velocity of the ablated material, compared to shorter pulses. Furthermore, longer pulses remove less material per pulse and therefore reduce the risk of damaging the target object more via ablation over time.

Regardless of the pulse length, each single laser pulse produces an unique impulse at the target. In conclusion, a higher pulse repetition rates allow for a more rapid deceleration. Doubling the pulse repetition rate, doubles the yield of angular momentum. This often allows for a better de-spinning performance than increasing the pulse energy or the surface fluence. Additionally the effectivity of increasing the surface fluence is capped by the maximum impulse coupling coefficient, shown in Figure 1. For de-spinning applications, a higher repetition rate enables an equally faster reduction of target rotation rates, provided sufficient electrical power is available on the servicing spacecraft. Consequently, the repetition rate should be selected as high as permitted by the servicer's power and thermal constraints.

In summary, spaceborne LIDAR lasers represent a technologically mature and space-qualified baseline for laser-ablative de-spinning systems. The exemplary calculations above show that the AEOLUS laser is well suited for de-spinning applications. Therefore, the development of novel laser systems is not necessary. The required pulse energies, durations, and repetition rates for laser ablation-based de-spinning are state of the art. This allows to leverages existing infrastructure to address the urgent need for debris mitigation, with minimal cost, risk, and development time. In Table 2, we provide a summary of the laser parameters suitable for laser ablation-based de-spinning in orbit to support future developments or modifications of laser systems.

Table 2: Suitable ranges of laser parameters for laser-ablative de-spinning in orbit. These are estimated values based on application feasible laser systems.

Parameter	Value Range	Reasoning
Pulse energy	$\geq 200\,\mathrm{mJ}$	A sufficient pulse energy is required to create ablation, even for large incidence angles and reflective surfaces. Ideally, the energy is sufficient to always create ablation with the highest possible impulse coupling coefficient.
Pulse duration	$1 - 100\,\mathrm{ns}$	The pulse length mainly influences the ablation mechanism (vaporization, spallation, phase explosion). For nanosecond pulses the ablation is predominantly caused by melting and vaporization. This reduces unnecessary mass ablation and provides a larger specific impulse.
Wavelength	$300 - 1500\,\mathrm{nm}$	The wavelength influences the absorption of the target material and therefore the impulse coupling coefficient. To date, measured impulse coupling coefficients are limited for different wavelengths and materials.
Pulse repetition rate	$> 50\,\mathrm{Hz}$	A higher repetition rate allows for a more rapid deceleration. Rates below $> 50\,\mathrm{Hz}$ are not recommended, since the de-spinning process becomes often time consuming
Beam quality	< 2	Relatively uncritical, provided the exit aperture is sufficiently large.

4. Simulation Framework

The developed simulation framework models the interaction between a pulsed laser system and a rigid body with a given angular impulse and corresponding angular velocity. The relative velocity between the laser system and the target body is fixed at zero. The primary goal of the software is to predict the impulse generated on the target for a given set of laser and material parameters. These predictions can be used to estimate the de-spinning time, power consumption of the servicer and can provide insights and restrictions for mission and servicer design.

4.1. Laser-Matter Interactions

The software employs the raytracing engine OptiX from Nvidia to simulate the laser beam as a bundle of rays. Within this bundle each ray carries a given fluence values based on the ray's location in the defined beam profile. For the current work the beam profile is defined as a Gaussian beam. The caustic of the beam is modeled using three distinct ray bundles, representing the converging, focused and diverging part of the beam. Each ray is propagated from the laser system on the servicer satellite to the target object. The intersection of each ray with the target surface is computed using a mesh-based geometric model of the target, where each surface of the mesh-model is assigned a material with a set of material parameters. For each ray, the generated impulse change $\Delta\vec{p}(\vec{r})$ is calculated based on the incidence angle, the distance between the laser and the intersection point $\vec{r}$, the laser and the material parameters. The calculation of the impulse

$$\Delta\vec{p}(\vec{r}) = -\hat{n}(\vec{r}) \cdot c_{\mathrm{m}}(\Phi_S(\vec{r})) \cdot \Phi_L(\vec{r}) \cdot dA_L(\vec{r}) \tag{5}$$

directly derives from the definition of the impulse coupling coefficient $c_{\mathrm{m}}(\Phi_S(\vec{r}))$ and further incorporates the geometric orientation of the impulse vector normal to the surface. Here, $\hat{n}(\vec{r})$ is the normal vector of the surface at the hit point, $c_{\mathrm{m}}(\Phi_S(\vec{r}))$ is the impulse coupling coefficient for the local surface fluence $\Phi_S(\vec{r})$, $\Phi_L(\vec{r})$ is the incident laser fluence at the hit point and $dA_L(\vec{r})$ is the area of the laser profile represented by a single ray. The total generated impulse for a single laser pulse is then calculated by accumulating the impulses of all N rays in the bundle.

$$\Delta\vec{p}_{\mathrm{shot}} = \sum_{i=0}^{N} \Delta\vec{p}(\vec{r}_i) \tag{6}$$

Ideally, the centre of mass of the target is placed in the origin of the used coordinate system. This simplifies the calculation of the generated angular impulse change $\Delta\vec{L}$ for a single ray to a cross product between the intersection point of the ray and the computed impulse, which is given by

$$\Delta\vec{L} = \vec{r} \times \Delta\vec{p}(\vec{r}). \tag{7}$$

Finally, the total angular impulse for a single laser pulse is again calculated by accumulating the angular impulses of all rays

$$\Delta\vec{L}_{\mathrm{shot}} = \sum_{i=0}^{N} \vec{r}_i \times \Delta\vec{p}(\vec{r}_i), \tag{8}$$

equally to the total impulse.

This provides the foundation to simulate the de-spinning of any target object, with known geometry, material properties and rotation state. In most cases, the required information is not known a priori for space debris objects. While the geometry and rotation state can be measured by the servicer satellite with minor uncertainties, the material properties are often completely unknown and have to be estimated using lab-based measurements. This introduces uncertainties in the simulation results. To optimize the simulation fidelity at mission time, the software includes the possibility for a controlled closed-loop operation. Measured changes of the target rotation state can be used to optimize the simulation parameters and reduce uncertainties. Therefore the base frame of the software not only aims for the simulation of laser-matter interactions but also includes principles of control theory to include in future servicer operations.

4.2. Optimization Process

Another foundation of the simulation framework focusses on the optimization of the irradiation spots on the target surface. By choosing suitable spots for laser ablation, the de-spinning time can be reduced significantly. Since the resulting angular impulse depends on multiple, partly dependent variables, a numerical optimization approach is

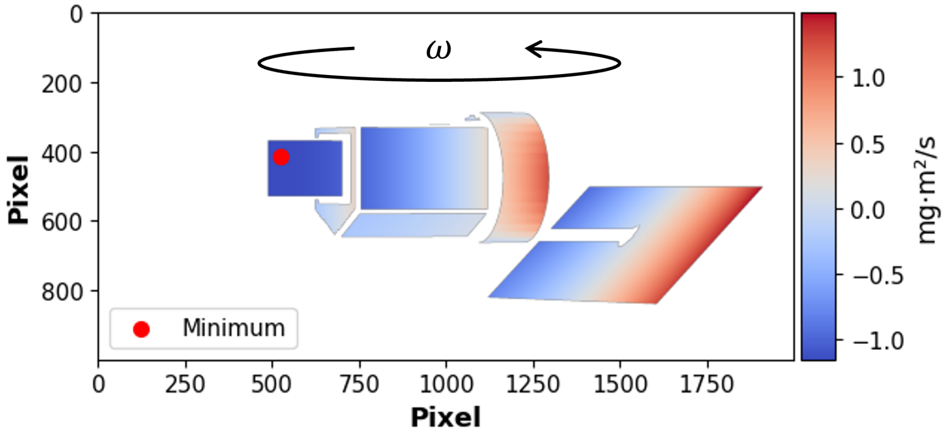

Figure 2: Example of the y-component of the resulting angular impulse on a spinning satellite. Spots that are further away from the centre of mass generate higher angular impulses.

chosen. Instead of simulating a single laser beam according to the user-defined parameters, multiple rays are traced from the laser system to multiple spots on the visible target surface. For each spot the resulting angular impulse is calculated and stored as an image map, like shown in Figure 2. By choosing spots with high angular impulse in the opposite direction of the current rotation, the de-spinning process can be accelerated. The pixel values are converted into a laser direction and the full beam profile and caustic are simulated for the chosen spot/direction. To further improve this optimization, multiple image maps based on different simulation results can be combined in a merit function. This merit function can be designed to optimize multiple objectives, create relations between different results or just simply weight them differently. An example merit function FOM could be defined as

$$FOM = w_1 \cdot L_y + w_2 \cdot \sqrt{L_x^2 + L_z^2} \tag{9}$$

Here, the merit function produces small (negative) values for spots that generate deceleration in y-direction and small angular impulses in the x- and z-direction. Therefore the resulting laser direction produces a high deceleration around the y-axis, while minimizing disturbances in the other two axes. The weights w_1 and w_2 can be used to prioritize one objective over the other. Furthermore, the merit function is represented as a 2D-image. This image can be optimized using image processing algorithms, e.g. a low pass filter kernel, which can smooth the merit function. The size of this filter kernel fitted to the beam pointing jitter of the laser and therefore incorporate the real-world random aiming error directly in the optimization. Morphological filters, like an erosion, can introduce a safety distance to restricted surfaces and guaranties a safe hit even with a beam pointing jitter.

4.3. Beam Pointing Jitter

The beam pointing jitter is not only estimated in the optimization process, but also modeled as a disturbance of the nominal laser direction. This disturbance is modeled using an Ornstein-Uhlenbeck-Process, which is a stochastic process with a tendency to return to a mean value. This mean value is the nominal laser direction defined by the optimization process. The Ornstein-Uhlenbeck-Process is defined by the stochastic differential equation

$$x_{k+1} = e^{-\frac{dt}{\tau}} \cdot x_k + \sigma \sqrt{1 - e^{-2\frac{dt}{\tau}}} \cdot \sigma \cdot N(0, 1) \tag{10}$$

Here, dt is the time step of the jitter model (typically smaller than the pulse repetition time), τ is the correlation time of the process, σ is the standard deviation of the process and $N(0, 1)$ is a normally distributed random number with mean 0 and standard deviation 1. By choosing suitable values for τ and σ, the beam pointing jitter can be modeled realistically. High values of τ produce slowly changing jitter, while low values produce fast changing jitter. The standard deviation σ defines the size of the jitter. At the moment, only the beam pointing jitter is modeled. For a disturbed beam direction, two angles are modeled in superposition to create varying beam vectors along the nominal beam direction.

With the Ornstein-Uhlenbeck-Process other disturbances can be modeled as well. E.g., a disturbance caused by heat is often slowly changing over time and can be modeled with higher values of τ. The challenge for future work is to identify suitable values for τ and σ for different disturbance sources and add them together to a complete disturbance model.

5. Demonstration of the Simulation Software

5.1. Simulation Setup

As a demonstration target an inactive US weather satellite, DMSP 5 D-2 F11 (Norad-ID: 21798), is chosen. A detailed description of this satellite can be found in Figure 3 published by the United States Air Force [13]. The surface of the satel-

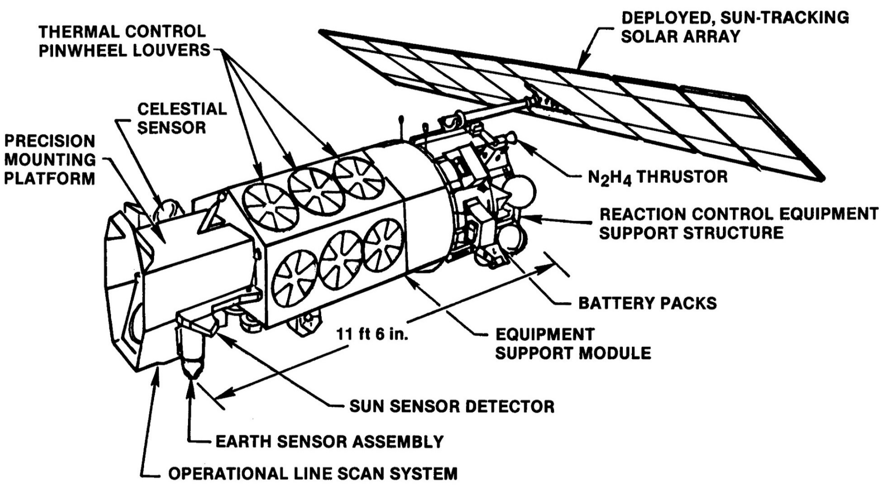

Figure 3: Shape and modules of a DMSP 5 D-2 satellite [13]. The satellite consists of a main bus structure with instruments, thrusters and support modules and a solar panel array.

lite was assumed to be aluminum, which is a common material for satellite structures. Additional surfaces of the satellite were defined as non-irradiable, e.g. solar panels, thrusters or edges with uncertain normal directions. These restricted surfaces are

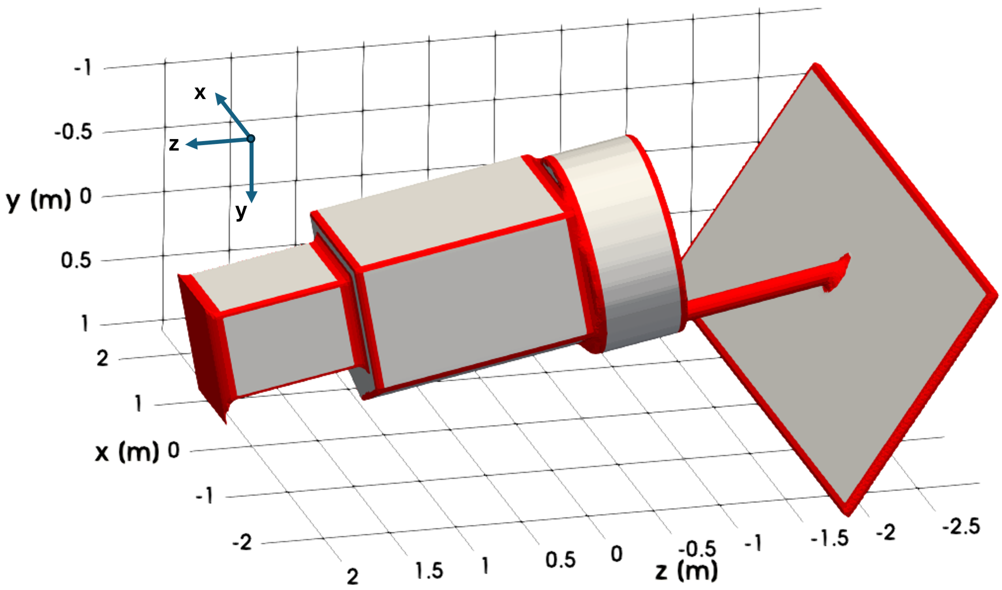

Figure 4: Geometry model of the DMSP 5 D-2 F11 satellite with the defined body frame. Gray surfaces are defined as aluminum and red surfaces are not allowed to be irradiated.

marked in red in Figure 4, while the aluminum surfaces are shown in gray. This geometry model is simplified compared to the real satellite, as small details like antennas, thrusters or other instruments are neglected. For a first feasibility study this simplification is acceptable, as the main structure of the satellite is represented well. Detailed geometry models can be acquired in-orbit using active scanning methods, which is out of scope for this paper. Additionally, the satellite manufacturer can provide a detailed model of the surface of the satellite to include all relevant details in the simulation. However, damages or other changes of the surface can occur over time and invalidate provided geometry models.

This satellite was measured by the Izaña station in Tenerife, Spain, and the data was evaluated by the DLR Stuttgart. The most recent measurement from September 2025 resulted in a rotation period of $7.6\,\mathrm{s}$. The axis of this rotation relative to the body frame is unknown and has to be assumed. One promising guess is a rotation around the principal axis with the smallest moment of inertia, which is the z-axis in this case. It has to be noted that the rotation axis can change over time by angle and magnitude. In-orbit perturbations like gravity gradient torques, solar radiation pressure or magnetic field interactions can change the rotation state of the satellite. However, for this feasibility study it is assumed that the rotation axis is constant over time. The body frame of the satellite is aligned with the estimated inertia frame. The estimation was made using a computer aided design (CAD) software with the assumption of a homogeneous density and a mass of $800\,\mathrm{kg}$. The following inertia tensor is estimated.

$$\mathbf{I} \approx \begin{bmatrix} 1500 & 0 & 0 \\ 0 & 1700 & 0 \\ 0 & 0 & 460 \end{bmatrix} \mathrm{kg\,m^2} \tag{11}$$

To achieve the rotation period of $7.6\,\mathrm{s}$ around the z-axis, the initial angular velocity vector is set to $\vec{L} = (0, 0, 380.3)\,\mathrm{kgm^2/s}$.

The laser parameters are chosen to approximate an optimized version of the Aeolus laser. The pulse energy is set to $420\,\mathrm{mJ}$ at a wavelength of $1064\,\mathrm{nm}$. Only the base frequency of the Nd:YAG laser is used to achieve higher pulse energies. The pulse length is $8\,\mathrm{ns}$ and the repetition rate is $50\,\mathrm{Hz}$. The beam is focused to a waist of $1.43\,\mathrm{mm}$ at a focus distance of $80\,\mathrm{m}$. The exit aperture of the laser system is placed with exactly this $80\,\mathrm{m}$ distance on the negative x-axis of the body frame. The laser system is assumed to have an exit aperture radius of $100\,\mathrm{mm}$. The relative velocity is always set to zero between servicer and target. It is assumed, that the the servicer controls the distance to the target and accelerates when both starting to drift apart.

5.2. Optimizing the De-Spinning Process

The simulation is run for a total of $7.6\mathrm{s}$, corresponding to one full rotation of the satellite. During this time, a total of 380 laser pulses are fired at the target. The optimization process determines the irradiation spots on the target surface for each pulse. In this preliminary study, only the nominal laser direction was used, without modeling beam pointing jitter.

For the optimization, two different merit functions are defined. The first merit function emphasizes on the reduction of the angular velocity around the z-axis with

$$FOM_1 = L_z + L_x^2 + L_y^2, \tag{12}$$

while only slightly punishing the creation of angular impulses around the x- and y-axis. The second merit function employs a higher cost factor for angular impulses around the x- and y-axis by modifying the weights w_1 and w_2, according to Equation 9. This results to the second merit function

$$FOM_2 = 10^{-3} \cdot L_z + 10^5 \cdot (L_x^2 + L_y^2). \tag{13}$$

The resulting angular impulse over a single revolution is shown in Figure 5 for both merit functions. With both merit functions the angular impulse around the z-axis is reduced constantly. However, the first merit function produces more angular impulse around the z-axis compared to the second merit function. This advantage comes at a cost. The first merit function produces significant angular impulses around the x and y-axis. Over time this irradiation strategy will produce an accelerating tumbling motion before capture conditions are met. By adding more weight to the angular impulses around the x and y-axis, the second merit function is able to remain a stable flat spin until capture conditions are met.

As demonstrated in [1], linear deceleration of a rotating space object can only be achieved under the condition of a continuous flat spin about a single principal axis. In this configuration, the irradiation spots on the target surface remain fixed relative to the body frame, enabling a simplified estimation of the de-spinning time based on a single rotation period. Small residual angular impulses about the x- and y-axes are neglected in this analysis, as they are assumed to have a negligible impact on the overall rotational dynamics.

To satisfy the requirements for robotic capture, the target's rotation rate must be reduced to below $4\,°/\mathrm{s}$. This corresponds to a final angular impulse of $32\,\mathrm{kg}\cdot\mathrm{m}^2/\mathrm{s}$. With an initial angular impulse of $380\,\mathrm{kg}\cdot\mathrm{m}^2/\mathrm{s}$ and a reduction of approximately $0.311\,\mathrm{g}\cdot\mathrm{m}^2/\mathrm{s}$ every $7.6\,\mathrm{s}$, the estimated de-spinning time is approximately $98.5\,\mathrm{days}$. This duration is

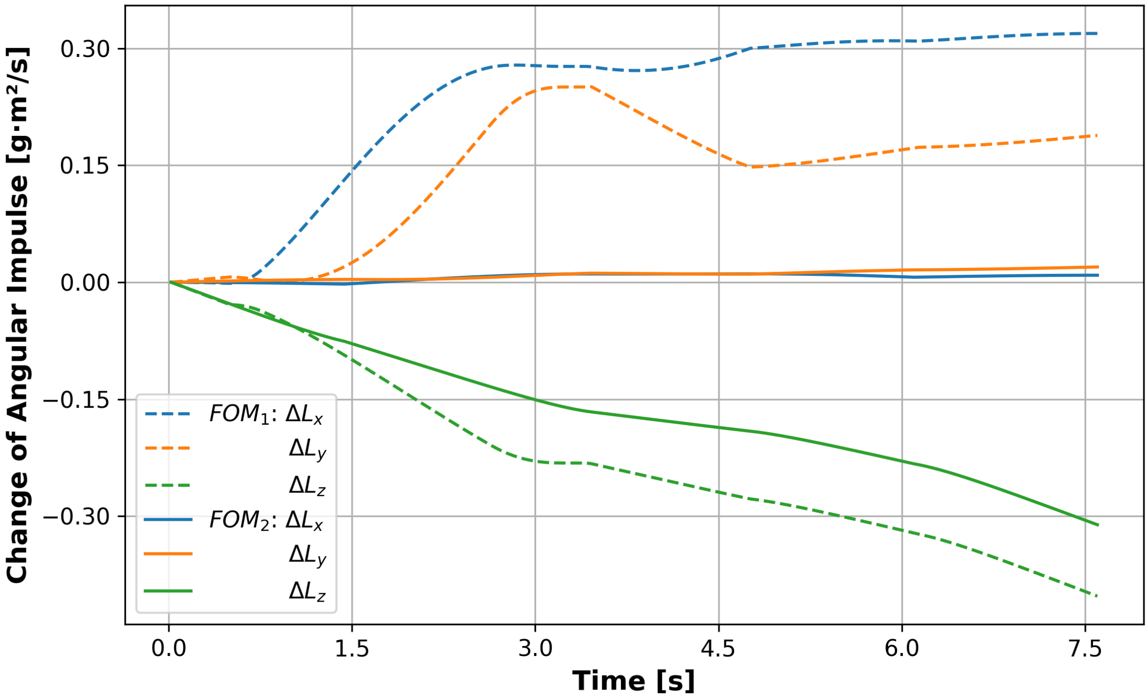

Figure 5: Angular velocity of the DMSP 5D-2 F11 satellite over time during laser-ablative de-spinning. The dashed lines represent the first merit function, while the solid lines represent the second merit function. Only the second merit function is able to remain a relatively stable flat spin around the z-axis.

deemed feasible for mission planning and represents a viable pathway toward achieving stable capture conditions.

Nonetheless, the de-spinning time can be significantly reduced through alternative strategies. One promising approach involves increasing the laser pulse repetition rate. For instance, raising the rate to $100\,\mathrm{Hz}$ would approximately halve the de-spinning time to $49\,\mathrm{days}$. However, this improvement comes at the cost of increased power consumption, which may impose practical limitations on the laser system's operational capacity.

Furthermore, an alternative control strategy involves the intentional introduction of a controlled tumbling motion. This secondary rotational mode enables the irradiation spots to be dynamically distributed across a broader range of surface regions. As a result, it could be possible that the new irradiable regions provided a higher torque, thus accelerating the de-spinning process for both the initial and the secondary induced tumbling modes. It is important to recognize that maintaining a stable flat spin does not inherently guarantee the fastest de-spinning performance. In certain cases, a more complex rotational state may provide superior efficiency and enable faster convergence to the capture-ready conditions required for robotic operations.

The performance of the two distinct merit functions is illustrated in Figure 6. The left panel presents the merit function from the first simulation, which prioritizes maximal deceleration about the z-axis. The right panel displays the merit function from the second simulation, which emphasizes the maintenance of a stable flat spin. In both cases, the global minimum of the merit function is identified and corresponds to the optimal laser ablation spot on the debris surface.

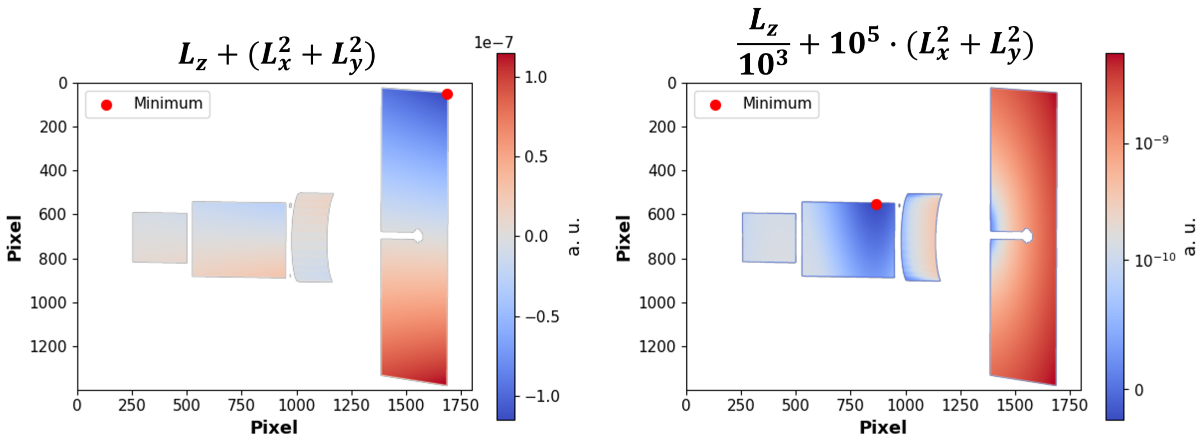

Figure 6: Comparison of the solutions of both merit functions for the target object after 2 s of rotation. Left: Merit function focussing on high deceleration around the z-axis. Right: Merit function focussing on stable flat spin.

The first merit function yields low values for locations farther from the center of mass, particularly favoring regions that generate substantial negative angular impulse along the z-axis. Angular impulses about the x- and y-axes are largely disregarded in this formulation, as they are not penalized enough in the objective function. Consequently, the selected ablation spots may induce non-negligible residual moments in the transverse directions, potentially leading to secondary rotational modes.

In contrast, the second merit function incorporates weights that strongly encouraging ΔL_x and ΔL_y values to remain close to zero. As a result the global minimum is located close to the x-y-plane, where the lever arm for ΔL_x and ΔL_y is zero. While this leads to significant lower angular impulses about the x- and y-axis, it also results in a slightly diminished deceleration around the z-axis due to a smaller lever arm. This is a trade-off that is necessary to maintain a stable flat spin.

This comparison demonstrates that the choice of merit function directly influences the resulting de-spinning behavior. By adjusting the weighting of different components in the objective function, the optimization process can be tailored to achieve specific dynamical outcomes. This flexibility underscores the importance of carefully designing the merit function to align with mission-specific requirements for robotic capture.

5.3. Introducing the Beam Pointing Jitter

In the preceding simulations, the nominal laser pointing direction is determined by the optimization process and was assumed to be perfectly realized. However, in a real-world scenario, the laser beam is inevitably subject to pointing jitter due to various perturbations, including mechanical vibrations of the servicer satellite, thermal deformations within the laser system, and inaccuracies in the beam steering mechanism. To assess the impact of such uncertainties on the de-spinning performance, the previously constrained ablation surface definitions were replaced with a uniform aluminum surface, enabling the evaluation of random irradiation spots across the target.

To model the beam pointing jitter in a physically consistent manner, the Ornstein-Uhlenbeck process, as detailed in Section 4.3, is employed. The parameters of the process, like the correlation time and standard deviation, are estimated based on the specifications of the laser system, augmented with a safety margin to account for unmodeled disturbances. For instance, the Aeolus laser system exhibits a beam pointing jitter of approximately $40\,\mu\text{rad}$, as described in [10]. In the current simulation setup, this corresponds to a spatial jitter of about $3.2\,\text{mm}$ at the target surface, assuming a target-servicer distance of $80\,\text{m}$.

To investigate the robustness of the de-spinning strategy under increasing jitter, a single revolution of the target was simulated. The laser pointing direction for each pulse was selected using the merit function FOM_2 defined in Equation 13. A series of simulations were conducted with progressively increasing standard deviations of the pointing jitter to quantify the resulting reduction in angular impulse per revolution. The outcomes are presented in Figure 7, illustrating the degradation of de-spinning efficiency as beam pointing uncertainty increases. These results highlight the critical importance of robust pointing control and error mitigation strategies in practical laser-based de-orbiting missions.

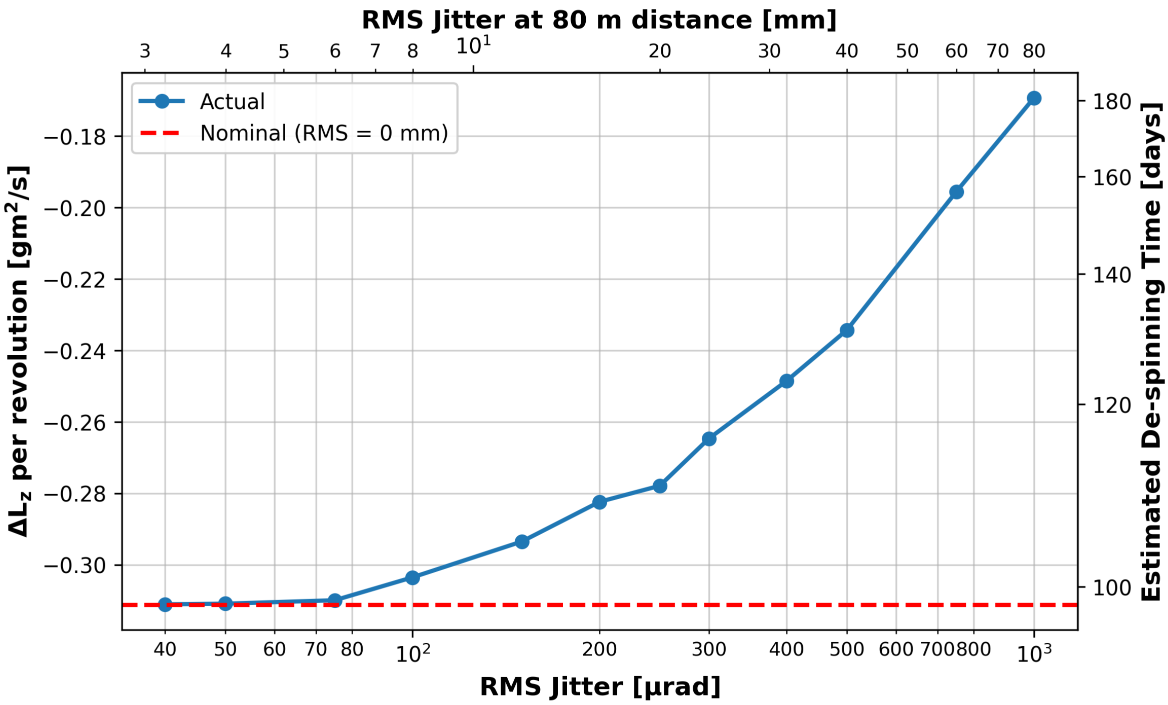

Figure 7: Reduction of the angular impulse around the z-axis per revolution for different values of the RMS of the beam pointing jitter. Increasing RMS values of the beam pointing jitter cause a significant slower deceleration of the target.

As the RMS value of the beam pointing jitter increases, the reduction in angular impulse is significantly diminished. However, for smaller RMS values below $75\,\mu\text{rad}$ or $6\,\text{mm}$ at the target surface, the resulting angular impulse stays close a nominal beam direction with zero jitter. Here, no significant reduction in de-spinning time is observed.

The significant increase in de-spinning time observed at elevated beam pointing jitter levels stems from a marked reduction in the effectiveness of angular impulse generation along the intended spin axis. As the pointing jitter intensifies, the laser beam increasingly strikes surface regions that either produce negligible torque or generate angular impulses in undesired directions. In extreme cases, ablation occurs at locations that induce angular momentum in the opposite direction to the intended de-spinning torque, effectively counteracting the deceleration effort. In some instances, the beam may even miss the target entirely, resulting in no momentum transfer at all.

This phenomenon is illustrated in Figure 8, which presents the evolution of angular impulse over a full target revolution under high jitter conditions. The top-left panel displays a rendered view from the laser's perspective, with the positions of previous laser impact points overlaid. The RMS pointing error is set to $1000\,\mu\mathrm{rad}$ to emphasize the disruptive effects of instability. A dense cluster of prior impact points is visible on the upper portion of the frontal surface, corresponding to effective torque generation and spin deceleration. The red cross marks the current laser hit location, which has been displaced upward due to jitter. Ablation at this position would generate a torque that accelerates the target's rotation about the z-axis, directly opposing the desired de-spinning objective.

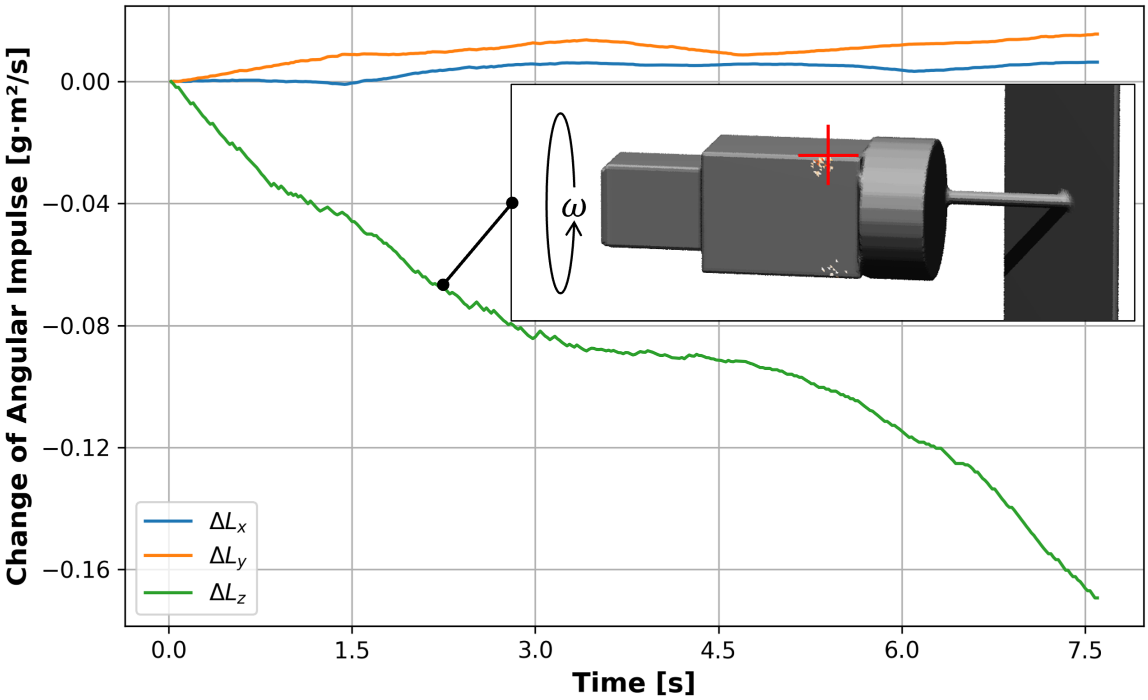

Figure 8: Change of angular impulse over the time of a single target revolution. Beam Pointing Jitter is visible in angular impulse characteristic and in the rendered image in the top-left corner. This image shows the target object, as well the the previous hit points as a light red colour. The red cross indicates the current laser hit point.

This counterproductive effect is further corroborated by a secondary cluster of prior hits near the lower edge of the frontal surface, which already contributes to unintended spin acceleration. The accompanying angular impulse profile clearly reflects this behavior, exhibiting small but distinct positive peaks corresponding to these unintended torques. These results demonstrate that beam pointing instability not only reduces the average torque magnitude but can also introduce periodic accelerations that degrade the overall de-spinning performance. This underscores the critical importance of precise beam pointing control in laser-based de-orbiting missions, particularly when aiming to achieve stable and efficient rotational damping.

By adding a padding of restricted zones at the edges of the geometry model such undesired accelerations or misses can be prevented. The size of the padding is determined by the RMS value of the pointing jitter. An alternative and complementary technique involves the application of image processing methods to the merit function. For instance, a low-pass filter with a kernel size proportional to the RMS jitter can be applied to smooth the merit function. This filtering operation averages the merit values over a spatial region corresponding to the expected beam footprint under jitter, effectively incorporating the uncertainty into the optimization. The resulting smoothed merit function prioritizes locations that are not only optimal in the nominal case but also robust against pointing errors, thus guiding the laser toward spots that remain favorable even when jitter is present. Together, these methods provide a systematic framework for enhancing the resilience of laser-based de-spinning systems to pointing errors, enabling more reliable and efficient operation in practical mission scenarios.

5.4. Estimated Power Consumption

Based on the simulated laser pulses sequence, the mean power consumption P_m of the laser system can be estimated, providing critical input for the design of the servicer's power supply. The mean power consumption P_m is calculated using the equation

$$P_m = \frac{E_{\mathrm{in}}}{\eta_{\mathrm{tot}} \cdot t_{\mathrm{tot}}}, \tag{14}$$

where E_{in} denotes the total laser energy delivered to the target, η_{tot} represents the overall laser efficiency, and t_{tot} is the total simulation time. The simulation yields a total energy irradiated at the target of $131.5\,\mathrm{J}$ per revolution. The total laser efficiency is estimated to be 0.2. Together with the total simulation time of $7.6\,\mathrm{s}$, the mean power consumption is estimated to be $86.5\,\mathrm{W}$.

6. Conclusion

This work presents a comprehensive investigation into the feasibility of laser-ablative de-spinning as a contactless method for enabling robotic capture of uncooperative space debris. The study combines a high-fidelity simulation framework with realistic modeling of operational uncertainties, demonstrating that rotational deceleration of fast-spinning objects is achievable within mission-relevant timeframes using existing spaceborne laser technologies.

The simulation framework, based on GPU-accelerated ray tracing and detailed beam caustic modeling, enables accurate prediction of momentum transfer by integrating empirically validated impulse coupling coefficients with geometric and material properties of target objects. The framework accounts for laser-matter interactions under varying conditions, including surface fluence, incidence angle, and material response, and supports multi-material target modeling and dynamic rotation state evolution.

A critical aspect of the analysis is the evaluation of beam pointing jitter, a dominant source of performance degradation in real-world operations. This jitter was modeled using an Ornstein-Uhlenbeck process, which captures the correlations and random fluctuations of the pointing direction. The results show that increasing jitter leads to a significant reduction in effective angular impulse change, with unintended accelerations arising from off-axis ablation. The simulation can be used to estimated the maximum allowed jitter level, ensuring insignificant performance degradation.

To enhance resilience, an adaptive optimization approach is employed, using merit functions that are designed based on the desired objectives. As shown, by incorporating multiple objective into the merit function and using arithmetic combinations, the optimization can be customized to meet specific requirements. This merit function translates multiple objective into a single comprehensive equation, allowing for a flexible and tuneable optimization process.

Furthermore, a comprehensive guide for suitable laser parameters is given. It is shown that already orbit-qualified laser systems exist that are suitable for laser ablation-based de-spinning. The guide also provides suitable ranges of laser parameters for future laser systems.

In summary, laser-ablative de-spinning is demonstrated as a viable, scalable, and operationally robust method for preparing fast-spinning debris for capture. The integration of realistic laser parameters, adaptive optimization, and uncertainty-aware simulation establishes a foundation for autonomous, closed-loop debris removal missions. The results provide critical input for servicer design, mission planning, and the development of digital twins for in-orbit operations, advancing the path toward sustainable spaceflight.

References

[1] D. Baral, Laser-Ablative De-Tumbling of Space Debris Objects, Master's thesis, University of Applied Sciences Darmstadt, 2025. Available at: https://elib.dlr.de/220391/.

[2] M. Vasile, A. Gibbings, I. Watson, J.-M. Hopkins, Improved laser ablation model for asteroid deflection, Acta Astronautica 103 (2014) 382–394.

[3] S. Scharring, J. E. Sinko, A. Sasoh, H.-A. Eckel, H.-P. Röser, Experimental determination of the impulse coupling coefficient - standardization issues, International Journal of Aerospace Innovations 3 (2011) 33–43.

[4] C. Phipps, M. Birkan, W. Bohn, H.-A. Eckel, H. Horisawa, T. Lippert, M. Michaelis, Y. Rezunkov, A. Sasoh, W. Schall, S. Scharring, J. Sinko, Review: Laser-ablation propulsion, Journal of Propulsion and Power 26 (2010) 609–637.

[5] S. Scharring, L. Eisert, R.-A. Lorbeer, H.-A. Eckel, Momentum predictability and heat accumulation in laser-based space debris removal, Optical Engineering 58 (2018) 011004.

[6] Joint Air Power Competence Centre, The JAPCC Journal, Edition 22, 2016. Accessed: 2026-02-24.

[7] S. Hancock, C. Mcgrath, C. Lowe, I. Davenport, I. Woodhouse, Requirements for a global lidar system: spaceborne lidar with wall-to-wall coverage, Royal Society Open Science 8 (2021).

[8] N. G. S. F. Center, Icesat geoscience laser altimeter system (glas): Science measurements, n.d. Accessed: 2026-01-14.

[9] C. A. Hostetler, Z. Liu, J. Reagan, M. Vaughan, D. Winker, M. Osborn, W. H. Hunt, K. A. Powell, C. Trepte, Cloud-Aerosol Lidar with Orthogonal Polarization (CALIOP) Algorithm Theoretical Basis Document: Calibration and Level 1 Data Products (PC-SCI-201), Technical Report 20250006623, NASA Technical Reports Server, 2025. Accessed: 2026-01-14.

[10] M. Endemann, The ADM-Aeolus mission, in: E. Armandillo, J. Costeraste, N. Karafolas (Eds.), International Conference on Space Optics — ICSO 2006, volume 10567, International Society for Optics and Photonics, SPIE, 2017, p. 1056701.

[11] D. Keil, S. Scharring, E. Klein, R.-A. Lorbeer, D. Schumacher, F. Seiz, K. Sharma, M. Zwilich, L. Schnörer, M. Roth, M. Ben-Larbi, C. Wiedemann, W. Riede, T. Dekorsy, Modification of space debris trajectories through lasers: Dependence of thermal and impulse coupling on material and surface properties, Aerospace 10 (2023) 947.

[12] S. Scharring, R.-A. Lorbeer, H.-A. Eckel, Numerical simulations on laser-ablative micropropulsion with short and ultrashort laser pulses, Transactions of the Japan Society for Aeronautical and Space Sciences 14 (2016). 10.2322/tastj.14.Pb_69.

[13] J. C. Wilman, U. States, Space Division: A Chronology, 1980–1984, AFSC Historical Publication, Office of History, Headquarters, Andrews Air Force Base, Md., 1991. Publication date uncertain; possibly 1991.